Gaussian Process Regression for Sensorless Grip Force Estimation of Cable-Driven Elongated Surgical Instruments

Yangming Li and Blake Hannaford

***Abstract*—Haptic feedback is a critical but a clinically missing component in robotic minimally invasive surgeries. This paper proposes a Gaussian process regression (GPR) based scheme to address the gripping force estimation problem for clinically commonly used elongated cable-driven surgical instruments. Based on the cable-driven mechanism property studies, and surgical robotic system properties, four different GPR filters were designed and analyzed, including one GPR filter with two-dimensional inputs, one GPR filter with three-dimensional inputs, one GPR unscented Kalman filter (UKF) with two-dimensional inputs, and one GPR UKF with three-dimensional inputs. The four proposed methods were compared with the dynamic model based UKF filter on a 10 mm gripper on the Raven II surgical robot platform. The experimental results demonstrated that the four proposed methods outperformed the dynamic model based method on precision and reliability without parameter tuning. And surprisingly, among the four methods, the simplest GPR Filter with two-dimensional inputs has the best performance.**

***Index Terms*—Sensorless grip force estimation, elongated cable-driven instrument, Gaussian process regression (GPR), surgical robot, minimally invasive surgery.**

I. Introduction

SURGICAL robots extended applications of minimally invasive surgery(MIS) by providing surgeons with improved freedom of movement, decreased hand tremor, increased accessibility and advanced 3-dimensional imaging [1], [2]. Haptic perception is still a missing component clinically [3] in robotic MISs, because of the challenge of the problem. However, haptic perception is highly desirable, because surgeons rely on it to diagnose and to adapt their motion to prevent unintended tissue damage or task failure.

The most straightforward way to perceive haptic force is to use sensors to directly measure the force on instrument tips. For minimally invasive surgery instruments, the stringent size, cost, and environmental requirements prevented the application of these techniques. Although various sensors broke the size limitation [4]–[6], they are still not widely available due to the cost, sterilization requirements and other factors. It is also possible to "indirectly" measure tip force through novel mechanical designs. For example, Tholey *et al.* designed a novel laparoscopic tool with tri-directional force measurement capability at the grasping jaws [7], and the disturbance observer was applied to estimate the force [8]. Zhao *et al.* proposed and developed a novel 3-DoFs robotic surgical tool to estimate tool-tissue forces through force-sensitive resistors [9]. These new designs are very useful, but they also increased the complexity and the cost, and haven't been widely adopted clinically. An in-depth discussion on the advantages and disadvantages of solutions to the force perception problem can be found in [3].

It is possible to achieve the active gripping force of a surgical instrument without adding sensors, since active gripping forces originate from motor output torques. For some deformable instruments, the interaction force can be estimated through measuring the instrument deformation. For example, Khoshnam *et al.* used the shape changes of the Steerable Ablation Catheters to estimate the contact forces between the catheter tip and cardiac tissue [10]. For rigid instruments, such as elongated grippers, motors drive cables and the output energy of motors is partially consumed by friction, converts to kinetic energy and forms the gripping force. Although it is clear that dynamic model describes the process of energy exchange and conversion, it is not trivial to apply this idea to the force estimation problem, as some of the factors mentioned above, such as friction and cable properties, are difficult to model. Friction is a phenomenon arising at the contact of surfaces, and experiments indicate a functional dependence upon a large variety of parameters, for example: sliding speed, acceleration, critical sliding distance, temperature, normal load, humidity, surface preparation, and material combination [11]. Anooshahpour *et al.* proposed a smart way to minimize the impact from the friction and from the movement by constructing the dynamic model of the da Vinci instrument under the quasi-static condition [12]. Research demonstrated that cable stretch and friction depend on cable properties [13]–[15]. Based on these studies, Li *et al.* applied the square root Unscented Kalman Filter to estimate the gripping force through incorporating cable properties, cable friction and cable-pulley friction into the dynamic model [16]. However, it has been found that as friction and cable properties have big weights in the model, the method is sensitive to the model parameters [16], which depend on both system configuration and environment. For example, model parameters change

Manuscript received September 10, 2016; accepted January 8, 2017. Date of publication February 8, 2017; date of current version March 10, 2017. This paper was recommended for publication by Associate Editor I. I. Iordachita and Editor K. Masamune upon evaluation of the reviewers' comments. This work was supported in part by the National Institutes of Health under Grant 5R21EB016122-02, in part by the National Science Foundation under Grant 1227406, and in part by the Korean Institute of Science and Technology (KIST, Dr. Hujoon project).

Y. Li is with the Department of Electrical Engineering, University of Washington, Seattle, WA 98195 USA (e-mail: ymli81@uw.edu).

B. Hannaford is with Departments of Electrical Engineering, Bioengineering, Mechanical Engineering, and Surgery, University of Washington, Seattle, WA 98195 USA (e-mail: blake@uw.edu).

Color versions of one or more of the figures in this letter are available online at http://ieeexplore.ieee.org.

Digital Object Identifier 10.1109/LRA.2017.2666420

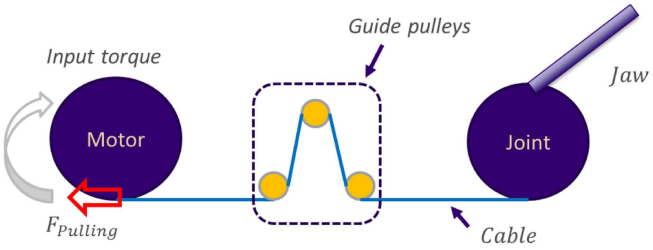

Fig. 1. Elongated cable driven surgical instrument model.

dramatically with instrument type and lubrication condition. Manually tuning these parameters for each instrument under various environmental conditions is very tedious and undesirable. Moreover, the effort [16] on on-line parameter estimation was not successful due to the fact that there are dozens of parameters and dozens of state variables and only 8 observations are generally available (4 motor torque outputs and 4 motor encoder readings for a wristed gripper).

In order to extend the application of the sensorless gripping force estimation to elongated cable driven surgical instrument, in this paper, we propose to simplify the estimation algorithm and to further improve estimation precision by learning the model from training data. Gaussian Process Regression was adopted in the paper because of its ability to deal with uncertainties and nonlinearity [17]. Four different designs of Gaussian Process Regression filters are proposed, and estimation precision will be compared on real surgical instruments and surgical robots. To sum up, the core contributions of the paper are:

1) We propose four Gaussian Process Regression filters, (which have no free parameters), for sensorless gripping force estimation, based on characteristics of elongated cable driven surgical instruments.
2) We implemented the proposed filters and applied them on a 10 mm gripper with the Raven-II robot;
3) We compared the four proposed methods with the dynamic model based UKF estimator on dry lab experiments with the real robot, validated the precision and reliability of the proposed methods, and identified the method of the best performance.

The paper is organized as follows: Section II presents preliminaries for the proposed methods; Section III explains the methods used for sensor-less force estimation in detail; Section IV presents and discussed the experiment setup and the experimental results. Conclusions are summarized in Section V.

II. Preliminaries

A. Elongated Cable Driven Surgical Instruments

Before presenting the proposed algorithms, we briefly introduce elongated cable-driven surgical instruments, discuss their properties, and show the reasons that data driven learning algorithms were adopted in the paper.

Motorized surgical instruments adopted the cable driven mechanism because of the advantages of easy sterilization, small size and narrow aspect ratio [18]. An example 10 mm diameter gripper can be seen in reference [16] Fig. 3. These cable-driven surgical instruments can be modeled as shown in Fig. 1.

The dynamic model describes how a instrument exerts force on an object and exchanges energy. The dynamic model can be mathematically expressed as:

$$\begin{aligned} \ddot{q} &= A^{-1}\left[\Gamma - H\left(q,\dot{q}\right)\right] \\ H\left(q,\dot{q}\right) &= C\left(q,\dot{q}\right) + G + \mathrm{diag}\left(\dot{q}\right)F_v \\ &\quad + \mathrm{diag}\left(\mathrm{sign}(\dot{q})\right)F_c + J^T F_{ex} \end{aligned} \tag{1}$$

where: A is the Inertia matrix of the manipulator; J is the Jacobian projecting external force into the reference coordinates; $C(\cdot)$ denotes the vector of Coriolis and centrifugal torques; G is the vector of gravitational force; $q, \dot{q}, \ddot{q}$ are the manipulator position, velocity and acceleration, respectively; F_v, F_c are viscous friction and coulomb friction parameters, respectively; and Γ, F_{ex} are joint input torque and external torque (gripping force in our application) respectively.

Because of the cable driven mechanism, the relationship between the motor and the joint can be described as:

$$\begin{aligned} \ddot{q}_m &= (1/A_m)(\Gamma - F_l - F_m) \\ F_l &= -r_m\gamma \\ \gamma &= k_e(f_{cs}(q_m, q_l, r_m, r_l)) + 2b_e(f_{cd}(\dot{q_m}, \dot{q_l}, r_m, r_l)) \\ F_m &= C_m\left(q_m, \dot{q_m}\right) + F_{cm}\mathrm{sign}(\dot{q_m}) + F_{vm}\dot{q_m} \end{aligned} \tag{2}$$

where: $q_m, \dot{q}_m, \ddot{q}_m$: denote motor position, velocity and acceleration, respectively; $q_l, \dot{q}_l$: denote link position and velocity; A_m: denote the diagonal motor inertia matrix; $C_m(\cdot)$ denotes the vector of Coriolis and centrifugal torques in motor coordinates; F_{vm}, F_{cm} are viscous friction and coulomb friction parameters, respectively; r_m, r_l: are capstan radius of motor and link, respectively; γ: is the cable tension. And $f_{cs}(\cdot)$ and $f_{cd}(\cdot)$ are the functions that describe the spring and damping effect, respectively. The explicit form of these two functions depend on cable properties [14], [16].

From (1) and (2) we can easily see that the total number of parameters (6 friction related parameters plus 3 cable properties related parameters for each link) is bigger than the total number of state variables (6 state space variables for each link). And both of them are much bigger than the total number of available observations (2 observations for each link). Given the complexity of the dynamic model, it was not trivial to tune these parameters without extra sensors. More importantly, our previous research shown that the parameters depend on the system configuration and environmental conditions [16]. Therefore, this work was inspired by these difficulties and aimed to increase the adoption rate by simplifying the technique.

B. Gaussian Process Regression

Gaussian Process Regression(GPR) is a form of supervised learning [17]. GPR is similar to Bayesian Linear Regression(BLR) (see [19, Ch. 3.3]) in the sense that both of them aim at probabilistically estimating the expected output Y_* given input X_* with respect to the training set (X, Y) under the Bayesian framework as: $p(Y_*|X_*, X, Y)$, where we denote the relationship between the input X and output Y as: $Y = f(X) + \omega$, $\omega \sim \mathcal{N}(0, \sigma_n^2)$. According to the Bayesian framework, we have $p(Y_*|X_*, X, Y) = \int p(Y_*|X_*, f)p(f|X, Y)df$. If we assume the prior of the model was $p(f)$, then the posterior of f given training data was $p(f|Y, X) = \frac{p(Y|X,f)p(f)}{p(Y|X)}$, and the likelihood $p(Y|X, f)$ can be inferred from the training data. For example, in the Bayesian Linear Regression case, since the state space function $f(X)$ was linear as $f(X) = X^T w$, we have

$Y|X, w \sim \mathcal{N}(X^T w, \sigma_n^2 I)$, where I was an identity matrix, X is a $n \times k$ design matrix and w is a $k \times 1$weight vector [19].

In contrast to BLR, Gaussian Process Regression uses kernels to represent the model, instead of explicitly adapting specific linear models. This kernel based scheme allows the data "speak" for themselves, which leads to the biggest difference between GPR and BLR. The power of GPR originates from the concept of Gaussian process and the kernel based learning scheme. A Gaussian process is a collection of random variables, any finite number of which follows a joint Gaussian distribution. A Gaussian process is completely specified by its mean function, $m(X)$, and covariance function K, as $f(X) \sim GP(m(X), K)$. Because of the definition of Gaussian Process, we have

$$\begin{bmatrix} Y \\ Y_* \end{bmatrix} \sim \mathcal{N}\left(0, \begin{bmatrix} K & K_*^T \\ K_* & K_{**} \end{bmatrix}\right)$$

Therefore, the prediction Y_* given the known data Y is $Y_*|Y \sim \mathcal{N}(K_* K^{-1} Y, K_{**} - K_* K^{-1} K_*^T)$, where

$$K = \begin{pmatrix} k(X_1, X_1) & \cdots & k(X_1, X_n) \\ \vdots & \ddots & \vdots \\ k(X_n, X_1) & \cdots & k(X_n, X_n) \end{pmatrix}$$

$K_* = (k(X_*, X_1) \cdots k(X_*, X_n))$, and $K_{**} = k(X_*, X_*)$ are all calculated according to the selected Gaussian Kernel. Kernel selection for the GPR will be discussed below. The kernel based learning scheme is another important reason that GPR suits nonlinear applications. In order to easily understand this difference, we can safely conclude that the advantage of GPR over BLR is similar to the advantage of Kernel based methods over the corresponding linear methods. However, this kernel based learning scheme limited the ability to "predict" if the prediction happens far away from seen data. Consequently, in GPR, it will produce high uncertainties with these predictions. In out applications, this can be seen as an advantage, because it is easy to achieve training data that covers the entire workspace, and if the prediction happens out of the range, it is better to let users know the prediction is not confident rather than being overconfident.

C. Unscented Kalman Filter

Unscented Kalman Filter addressed the linearization approximation problem of the Kalman Filter with the unscented transformation [20]. For the nonlinear state space function $Y = f(X)$, assume X is L dimensional and had mean $\mathbf{E}(X)$ and covariance P, a $L \times (2L+1)$matrix composed of $2L+1$ sigma vectors χ_i formed with corresponding weights W_i:

$$\begin{aligned} \chi_0 &= \mathbf{E}(X) \\ \chi_i &= \mathbf{E}(X) + \left(\sqrt{(L+\lambda)\mathbf{P}}\right)_i, i = 1, \cdots, L \\ \chi_i &= \mathbf{E}(X) - \left(\sqrt{(L+\lambda)\mathbf{P}}\right)_{i-L}, i = L+1, \cdots, 2L \end{aligned} \quad (3)$$

$$\begin{aligned} W_0^m &= \frac{\lambda}{L+\lambda} \\ W_0^c &= \frac{\lambda}{L+\lambda} + (1 - \alpha^2 + \beta) \\ W_i^m &= W_i^c = \frac{1}{2(L+\lambda)}, i = 1, \cdots, 2L, \end{aligned} \quad (4)$$

and $\lambda = \alpha^2(L+\kappa) - L$ is a scaling parameter controlled by empirically determined parameter α and κ. The sigma points then are propagated through the nonlinear state space function to calculate the corresponding outputs $\gamma_i = f(\chi_i), i = 0, \cdots, 2L$, which are used to recover the posterior estimation.

The Gaussian Process Regression and the Unscented Kalman Filter were adopted in the paper because:

1) It is easy to get the training data for our application.
2) Gaussian Process Regression has outstanding ability to learn models for strongly nonlinear applications.
3) Gaussian Process Regression naturally estimates uncertainties, which is very important to increase the system ability of the teleoperation haptic feedback system.
4) It is not necessary to manually tune parameters of Gaussian Process Regression in our application.
5) Unscented Kalman Filter has outstanding ability to handle nonlinearity problem.
6) Unscented Kalman Filter does not require the derivatives of the model, only propagating sigma point is needed, therefore, it can be easily combined with GPR.

III. Gaussian Process Regression for Sensorless Grip Force Estimation

A. Gaussian Process Regression Force Estimation

Designing Gaussian Process Regression filters depends on the selection of the feature space. For motorized surgical instruments, motor encoder readings and motor output torques approximated by current sensing are always available. Therefore, naturally, encoder readings and output torque could be the inputs to the Gaussian Process Regression filter, and the gripping force should be the output. Mathematically, by following the denotations in Section II-B, we have $X = \{q_m, \Gamma\}$ as the training input data and $Y = \{F_{ex}\}$ as the output data. q_m, Γ and F_{ex} are explained in (1) and 2. $D = \{X, Y\}$ then is the training data.

The dynamic model of the elongated surgical instrument, which was mathematically explained in (1) and (2), suggests that the gripping force not only depends on motor position and motor output torque, but also depends on motor velocity $\dot{q_m}$, joint position q_l, and joint velocity $\dot{q_l}$. Therefore, the feature space formed by these variables should be better than the space formed only by q_m and Γ. Consequently, the estimation precision should be improved [17], [21]. However, the joint position and velocity are not observed in the process due to the lack of external sensors, and their estimation depend on cable properties [14], [22]. As one of the goals of this work is to explore the possibility of avoiding manually tuning cable parameters, we consider q_l and $\dot{q_l}$ as unavailable. On the other hand, the motor velocity $\dot{q_m}$ could be considered as available, because the motor encoders of our surgical robot produce high precision output, and with a simple filter, such as a Kalman Filter, the velocity can be easily estimated, as shown in Fig. 2. From the figure we can see that the raw observation and the integration of estimated velocity are almost identical (approximately delayed for one sampling period), which suggests we achieved desirable estimation precision. However, we know the velocity estimation directly depends on the position observations. Therefore, theoretically, the position observations have been used twice and may cause the overconfidence problem.

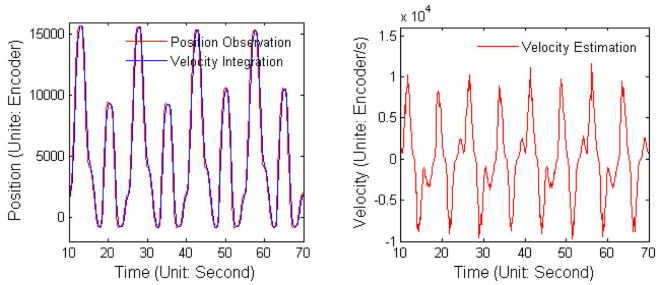

Fig. 2. Motor velocity estimated with Kalman filter based on position observation.

The next step of the proposed methods was to select the proper kernel function and the corresponding parameters. In the proposed methods, the popular widely used squared exponential kernel was adopted, because clear physical meanings for each parameter can be found in our application. The kernel is defined as: $k(X, X') = \sigma_f^2 exp(-\frac{1}{2}(X - X')^T M(X - X')) + \sigma_n^2 \delta(X, X')$, where $\delta(X, X')$ is the Dirac delta function defined as: $\delta_{ij} = \begin{cases} 1, & \text{if } i = j \\ 0, & \text{if } i \neq j \end{cases}$. And $M = l^{-2} I$, where l is a vector of positive values. In the model, l is the characteristic length-scale. In the proposed methods, l is small ($l = 1.2$ in the experiments) because it is easy to get training data and we have high resolution in the range of workspace. And σ_f and σ_n correspond to the process noise and the observation noise, respectively. In the proposed methods, σ_f and σ_n are selected bigger than the real dynamic model noises, ($\sigma_f = 0.3, \sigma_n = 0.6$ in the experiments) in order to safely "learn" from the training data. The process noise model depends on the system properties. For the gripper controlled by Raven II robot, from referenc [14] we know $0.3X3$ radian is far bigger than the true process noise. The observation noise model depends on the measurement sensor property, and the measurement noise of the sensor we adopted can be found in reference [16] Fig. 11. Please notice GPR does require normalizing features into similar ranges, just like other learning algorithms do, therefore, if the range of features change dramatically, these values should be changed accordingly. The experiments shown both the adopted kernel and the initial parameters worked well, mainly due to the good continuity.

B. UKF and Gaussian Process Regression Force Estimation

In Section II-C we mentioned that UKF avoids explicitly linearizing the state space function through the introduction of the concept of sigma points. This new feature increases its robustness against strong nonlinearity and the poor priors. It has been reported that UKF can be combined with GPR, and the results outperformed the classical dynamic model based UKF in blimp tracking [23]. It was interesting to test if the combination of UKF and GPR can outperform GPR on precision for the gripping force estimation problem.

Applying GPR to UKF was simple. In the training phase, there is no difference between the GPR and the GPR based UKF, they share the same GPR and use the exactly same learning scheme. In the estimation phase, the GPR based UKF produce $2L + 1$ sigma points according to (4). And $2L + 1$ estimations, denoted as γ_i, are generated through passing the sigma points through the trained GPR. The posterior of estimation can be recovered

Algorithm 1: UKF&GPR for Grip Force Estimation.

Train GPR with training data (X, Y)
Calculate sigma points $\chi_{t-1} = \{\chi_{t-1,i}\}, i = 0, \cdots, 2L$ of X_*, according to (4)
$P_{t|t-1} = P_{t-1} + Q_t$
for $i = 0, \cdots, 2L$ **do**
  Calculate $\gamma_{t-1,i} = GP(\chi_{t-1,i})$
end for
$Y_* = \sum_{i=0}^{2L} W_i^m \gamma_i$
$P_t = \sum_{i=0}^{2L} W_i^c (\gamma_i - Y_*)(\gamma_i - Y_*)^T$

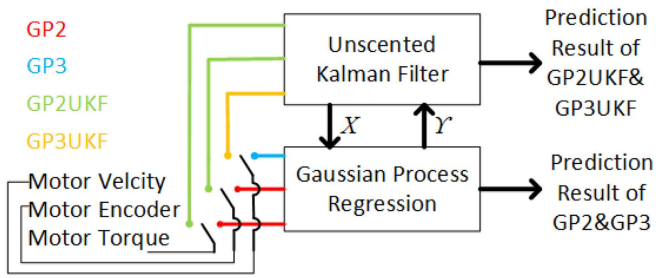

Fig. 3. Gaussian process regression for elongated cable-driven surgical instrument sensorless grip force estimation.

from γ_i as:

$$\mathbf{E}(Y) = \sum_{i=0}^{2L} W_i^m \gamma_i$$

$$P = \sum_{i=0}^{2L} W_i^c (\gamma_i - \mathbf{E}(Y))(\gamma_i - \mathbf{E}(Y))^T,$$

where the weights W^m and W^c are calculated according to (4), and the covariance P is calculated for generating sigma points at the next time point. The pseudocode of the GPR based UKF was listed in Algorithm 1.

Through the discussion we know that because of the selection of different learning scheme and feature spaces, we have four GPR based filters for the sensorless gripping force estimation problem. Firstly, we can use two types of inputs. One is two dimensional and is composed of motor torque and motor encoder, and the other one is 3-dimensional and is composed of motor torque, motor encoder and motor velocity. Secondly, we have two types of estimator architectures. One is the classical GPR and the other one is the GPR based UKF. The difference between the two is the GPR based UKF uses GPR as the dynamic model. The combination of two input types and two architectures leads us to four estimators. For simplicity, we refer to the GPR with two dimensional inputs as GP2, the GPR with three dimensional inputs as GP3, and the GPR based UKF with two dimensional inputs as GP2UKF, the GPR based UKF with the three dimensional inputs as GP3UKF. For clarity, the differences among the four types of estimators are also visualized in Fig. 3.

IV. Experimental Result and Discussion

The four proposed methods were implemented and compared with the dynamic model based estimator on a 10 mm diameter, cable-driven surgical gripper (can be seen in reference [16]

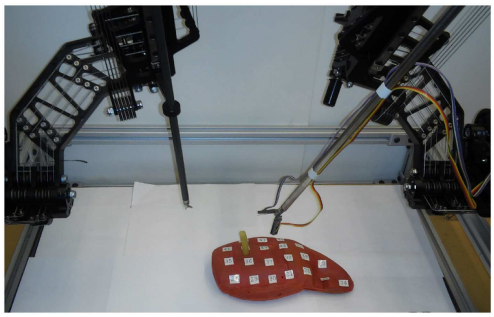

Fig. 4. Sensorless force estimation experiment setup. A 10 mm diameter, cable-driven surgical gripper was equipped with two force sensors (FSS015WNSB, Honeywell) on each of the two jaws. The gripper was driven by Raven II surgical robot and moved repeatedly and grasped a flexible latex rubber tube, which simulates blood vessel.

Fig. 3) on the Raven-II surgical robot. The Raven-II robot was also fully driven by cables. This paper focused on the instrument gripping force estimation. Therefore, in the experiments reported here, the Raven manipulator held still and only the instrument moved. The experimental platform can be seen in Fig. 4

Two force sensors (FSS015WNSB, Honeywell) were mounted on the tip of the gripper to directly measure forces, as shown in reference [16] Fig. 3. Two aprons that rotated with respect to the jaw joint were added to the gripper in order to eliminate uncertainties from movable contact position. The gripper was statically calibrated with weights that range from 0N to 2N, and linear fit results were:

$$\begin{cases} F_{left} = 0.07V_{left} + 0.04 \\ F_{right} = 0.07V_{right} + 0.18 \end{cases} \quad (5)$$

Detailed calibration information and usage can be found in [16], [24]. The gripping force was defined as the contact force between the object and the gripper jaw, which matches the sensor measurements. Given the definition, we know that the two forces on the left jaw and the right jaw are not equal, because of gravity, unsymmetrical contacting position and other factors.

A. Zero Grip Force Estimation Study

The proposed method was first verified with zero gripping force: the jaws repeatedly opened and closed, without touching each other or any other objects. Sensor measurements were compared with estimation results, while we know the true ground truth was nearly zero everywhere. The results are visualized in Fig. 5. The statistical results are compared in Table I. The results clearly show that estimations from both the four proposed methods and the dynamic model based method were smoother than sensor measurements, and the mean, the standard deviation, the threshold of 99% of data and the maximum error of the four proposed methods were very close to each other and outperformed the dynamic model based method. The results also shown the sensor measurements were noisy. A commercial force sensing unit, such as ATI Nano, are less noisy, but as we need to verify the proposed method in real movements, the instrument tips can be be fixed to a sensing unit. An alternative way is to estimate contacting position on-line, and convert torque to contact force. The current setup is chosen because: 1, the precision of estimating contacting point; 2, gripping a non-rigid object (rubber tube in our experiments) is preferable, as it better simulates real surgeries; 3, measurement error is high spikes and can be easily filtered out. An uncertainty based smoothing method was adopted to remove error spikes [25].

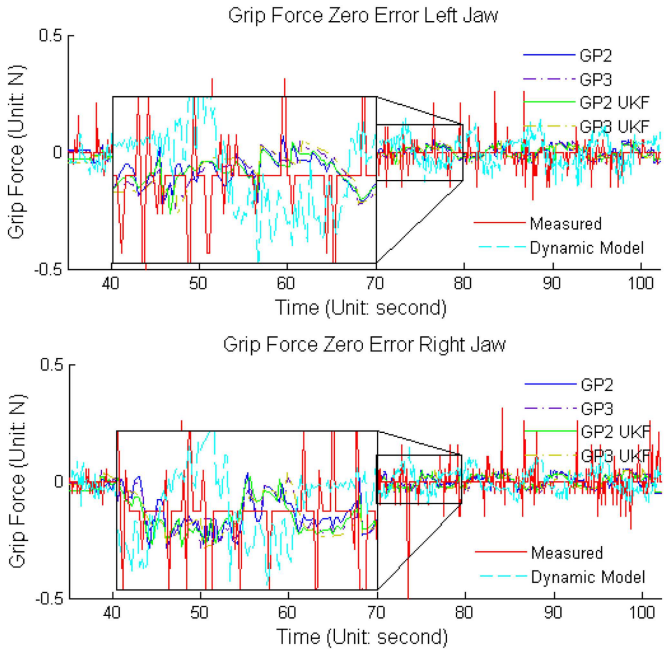

Fig. 5. Non-gripping sensor measurement and estimation results comparison. The jaws move without touching any objects, therefore, the gripping force should be very close to zero.

TABLE I
ESTIMATED AND MEASURED ZERO GRIP FORCE ERROR COMPARISON

		Averaged (Unit:N)	SD (Unit:N)	99%Value (Unit:N)	Max (Unit:N)
Sensor Measured	Left	0.02	0.05	0.15	0.51
	Right	0.02	0.05	0.16	0.60
Dynamic Model	Left	0.05	0.03	0.12	0.15
	Right	0.04	0.03	0.09	0.16
GP2	Left	0.02	0.02	0.04	0.05
	Right	0.02	0.02	0.04	0.05
GP3	Left	0.02	0.02	0.04	0.05
	Right	0.02	0.02	0.04	0.05
GP2UKF	Left	0.02	0.02	0.04	0.05
	Right	0.02	0.02	0.04	0.05
GP3UKF	Left	0.02	0.02	0.04	0.05
	Right	0.02	0.02	0.04	0.05

Note: SD: Standard Deviation; 99% value: the threshold of 99% of data.

B. Non-Zero Grip Force Estimation Study

The proposed method was verified while the gripper actually grasped an object in the teleoperation mode, as shown in Fig. 4. The gripper repeatedly gripped a 10 mm diameter flexible latex rubber tube, simulating the common blood vessel gripping operation. The entire gripping process runs at 10 Hz and continuous 50 seconds of data was used to train the proposed methods. The proposed methods were verified with about 40,000 data points, in which the gripper jaws moved between $-0.87 \sim 1.39$ radian at angular speed up to 0.57 radian/sec, and the wrist

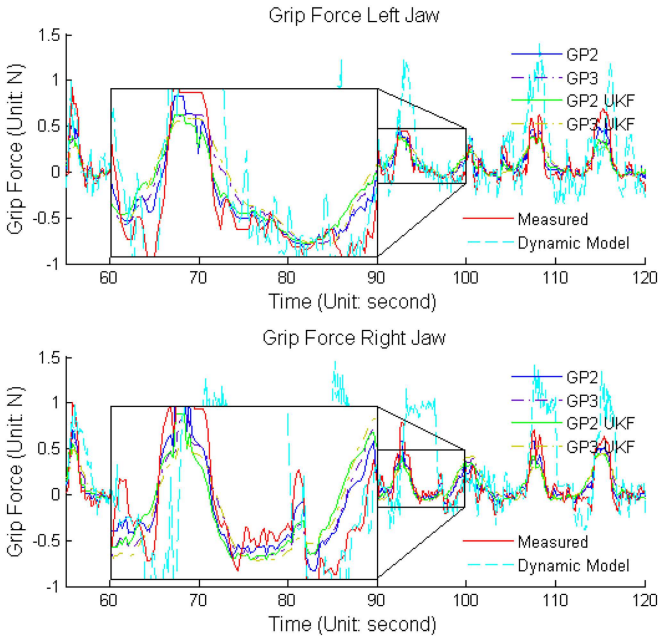

Fig. 6. Comparison among sensor measured force and estimation results from the four proposed method and the dynamic model based method.

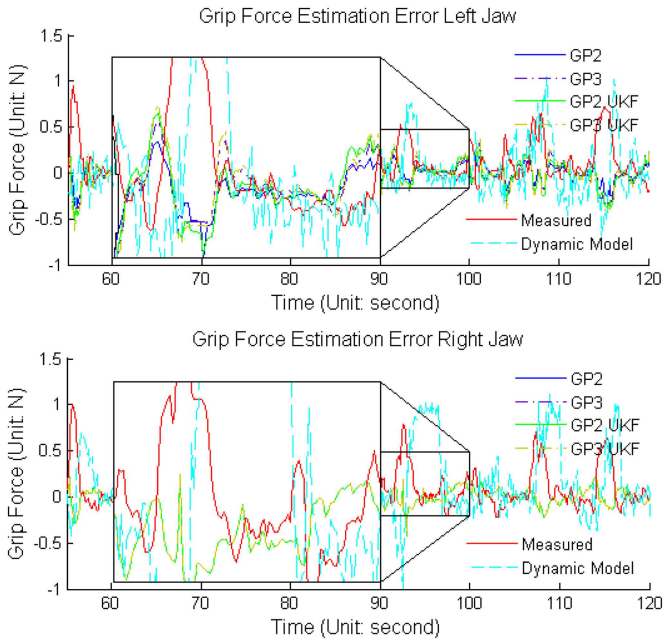

Fig. 7. Sensor measurement and estimation error comparison. Ground truth (sensor measurements) is shown with force estimation errors. Vertical axis label for the red line is grip force and for rest of the lines, vertical axis is force error.

moved between $-0.87 \sim 0.87$ radian at angular speed up to 0.75 radian/sec.

The comparison among the sensor measurements and the estimation results from the four proposed methods and the dynamic model based method was shown in Fig. 6. The results shown all four proposed methods outperformed the dynamic model based method on precision.

The difference between the sensor measurements and the estimation results from the four proposed methods and the dynamic model based method were compared with measured gripping force (red line) in Fig. 7. This was to show if the proposed filters caused delay on estimation results and to visualize where the maximum estimation error occurred. Unlike the dynamic model based method, GPR based methods did not have clear delay, even when UKF was adopted. But GPR based UKF (GP2UKF and GP3UKF) were conservative on estimation in the sense that the maximum estimation errors were always around the peak of measured forces. Please notice as the sensor measurements were compared with estimation errors, the y-axis in Figs. 6 and 7 share the same order.

The statistical results, including averaged, $99th$ percentile, and maximum differences, as well as the standard deviation, are shown in Table II. These results shown that the proposed methods had good precision of gripping force estimation and outperformed the dynamic model based method [16], even though no extra sensor or equipment was used.

One of the advantages of Gaussian Process Regression is it naturally generates uncertainty estimation. This is especially important to surgical force estimation since safety is the top priority in surgeries. All estimation results and uncertainties were compared with sensor measurements in Figs. 8 and 9. In the figures, the gray area shown the 99% confidence ($3 \times$ standard deviation) and the green lines shown the estimation. The uncertainties estimated by the proposed methods are comparatively high, which suggested that in our experiments, the data repeatability is low. In another word, different gripping forces are associated with similar input torque, motor position and velocity. This indicates the selected feature spaces do not have enough resolution for pattern recognition. Fine tuning the robot to make sure its tension, friction condition and other factors may decrease the uncertainties, however, it is difficult.

TABLE II
ESTIMATION ERROR COMPARISON

		Averaged (Unit:N)	SD (Unit:N)	99%Value (Unit:N)	Max (Unit:N)
Dynamic Model	Left	0.19	0.20	0.66	1.06
	Right	0.28	0.30	0.86	1.15
GP2	Left	*0.07*	*0.10*	*0.23*	*0.46*
	Right	*0.07*	*0.11*	*0.22*	0.56
GP3	Left	0.10	0.14	0.32	0.53
	Right	0.10	0.13	0.26	*0.54*
GP2UKF	Left	0.11	0.14	0.31	0.52
	Right	0.11	0.15	0.29	0.56
GP3UKF	Left	0.12	0.17	0.38	0.63
	Right	0.13	0.16	0.32	0.54

Note: SD: Standard Deviation; 99% value: the threshold of 99% of data

The histograms of χ^2 errors of the four proposed methods were compared with the χ^2 distribution to show if the mean and uncertainty really follow the normal distribution or not, and also to show how the errors are distributed (Figs. 10 and 11). From these figure we can see the estimation results from the four proposed method follow the corresponding χ^2, which is a sign indicating good robustness. The numerical difference between the χ^2 errors and the corresponding χ^2 distribution were compared in Table III. From the table we can see, agreeing with the precision results, the GP2 has the best similarity between the histogram and the distribution.

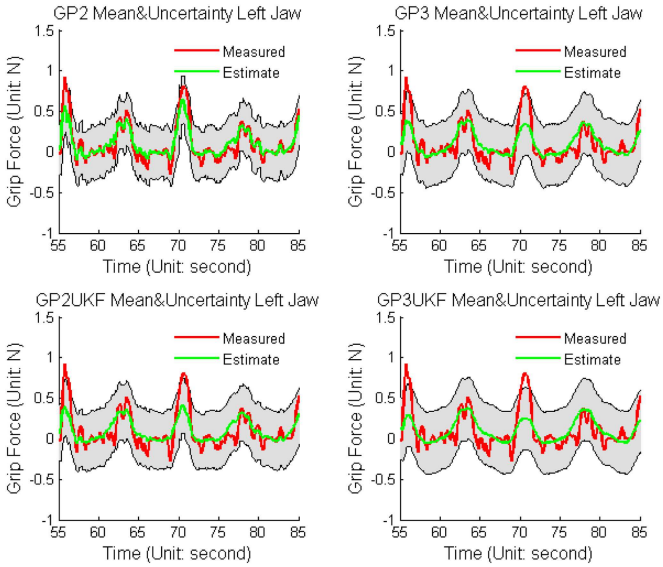

Fig. 8. Sensor measurement and GPR mean and uncertainty comparison for left jaw.

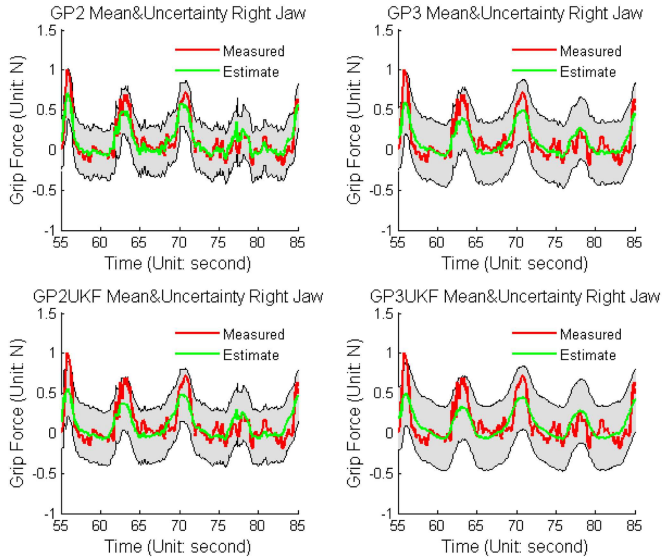

Fig. 9. Sensor measurement and GPR mean and uncertainty comparison for right jaw.

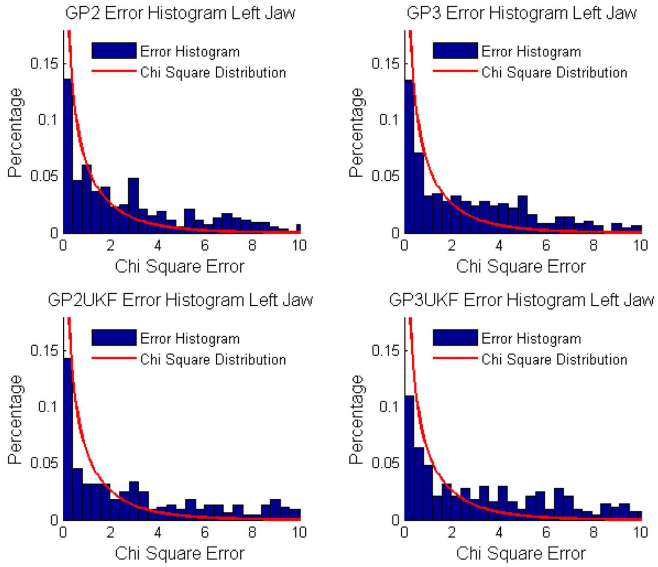

Fig. 10. χ^2 error and distribution comparison for left jaw force estimation. The similarity between the histogram and the curve showd the precision of uncertainty estimation.

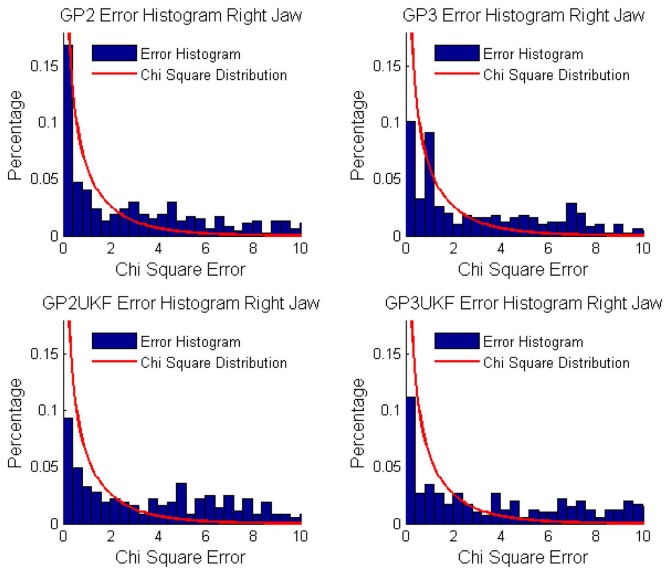

Fig. 11. χ^2 error and distribution comparison for right jaw force estimation.

TABLE III
χ^2 ERROR AND DISTRIBUTION NUMERICAL COMPARISON

	GP2	GP3	GP2UKF	GP3UKF
left	0.02	0.02	0.02	0.02
right	0.02	0.02	0.02	0.03

C. Analysis and Discussion

The experimental results demonstrated that the Gaussian Process Regression estimators outperformed the dynamic model base UKF estimator on precision for the sensorless gripping force estimation problem, which suggests that GPR suits our application. The GPR estimators proposed in the paper also provided uncertainty estimation as a side product, which would be useful because we will fuse force estimation results from multiple sources to further improve estimation precision and stability in our future work.

Table II indicated that among all four estimators, GP2 had the best force and uncertainty estimation. If we take a closer look at Figs. 6, 7, 8 and 9 we can find that GPR based UKF estimators tended to be more "conservative" than the GPR estimators, as they generated smoother estimations, which also caused the force peak values to be far away from the sensor measurements. In teleoperated surgical systems, the smoothness may be preferable because it increases the systematic stability. However, Figs. 10 and 11 demonstrated that the smooth

estimations from GP2UKF and GP3UKF have less similarity to the χ^2 distribution, which indicated the inconsistency between the mean and uncertainty estimation.

Experimental results also shown that, although the precision difference between GP2 and GP3, and between GP2UKF and GP3UKF are not huge, GP2 and GP2UKF were still slightly better. It is possible that this is due to the fact that the velocity estimation from position observations not only probabilistically depended on the position observation, but also introduced extra delay since we adopted a causal low pass filter. However, it may also suggest that GPR had very strong power to overcome the nonlinearity.

The computational complexity of GPR was thoroughly analyzed in [17]. In the proposed methods, the estimators trained with hundreds of data points, which made the computational complexity trivial to modern computers. As for the proposed estimators, it was clear GP3UKF had highest computational complexity, and GP2UKF was higher than GP3, while GP2 had the lowest complexity.

V. Conclusion

GPR based estimators were proposed to address the sensorless gripping force estimation problem for elongated cable driven surgical instruments. Compared to explicitly modeling the system, GPR has the advantages that it learns from data, is simple, and naturally generates estimation uncertainties. The four estimators were proposed and designed based on our study of surgical instrument properties and cable characterization. The proposed methods were compared with the dynamic model based estimator on a 10 mm gripper on the Raven II surgical robot. Experimental results demonstrated that the GPR estimators outperformed the dynamic model based estimator in the application, and among the four estimators, the simplest, GP2, had the best estimation precision and reliability. The results suggested that the proposed GPR with 2-dimensional inputs best fitted our application.

Next, the proposed method needs to be combined with teleoperation consoles to close the haptic feedback loop and to verify that the technique meets clinical needs. We also need to explore the usage of long-term learning [26] to improve the adaptiveness of the proposed method. Moreover, combining the GP2 estimator with other force estimation techniques, such as estimations of contacted tissue deformation, also attracts us. These extra information may be able to form a better feature space and achieve higher estimation precision and reliability. We also have the option to directly combine the GPR estimation results with those estimation techniques, through utilizing the uncertainty estimation of GPR and further improve estimation precision and reliability.

References

[1] M. J. Mack, "Minimally invasive and robotic surgery," *JAMA*, vol. 285, no. 5, pp. 568–572, 2001.

[2] P. Gomes, "Surgical robotics: Reviewing the past, analysing the present, imagining the future," *Robot. Comput.-Integrated Manufacturing*, vol. 27, no. 2, pp. 261–266, 2011.

[3] P. Puangmali, K. Althoefer, L. D. Seneviratne, D. Murphy, and P. Dasgupta, "State-of-the-art in force and tactile sensing for minimally invasive surgery," *IEEE Sensors J.*, vol. 8, no. 4, pp. 371–381, Apr. 2008.

[4] F. L. Hammond, R. K. Kramer, Q. Wan, R. D. Howe, and R. J. Wood, "Soft tactile sensor arrays for force feedback in micromanipulation," *Sensors J.*, vol. 14, no. 5, pp. 1443–1452, May 2014.

[5] S. K. Prasad *et al.*, "A modular 2-dof force-sensing instrument for laparoscopic surgery," in *Medical Image Computing and Computer-Assisted Intervention*. New York, NY, USA: Springer, 2003, pp. 279–286.

[6] M. Vatani, E. D. Engeberg, and J.-W. Choi, "Force and slip detection with direct-write compliant tactile sensors using multi-walled carbon nanotube/polymer composites," *Sensors Actuators A: Phys.*, vol. 195, pp. 90–97, 2013.

[7] G. Tholey, A. Pillarisetti, W. Green, and J. P. Desai, "Design, development, and testing of an automated laparoscopic grasper with 3-d force measurement capability," in *Medical Simulation*. New York, NY, USA: Springer, 2004, pp. 38–48.

[8] S. Katsura, Y. Matsumoto, and K. Ohnishi, "Modeling of force sensing and validation of disturbance observer for force control," *IEEE Trans. Ind. Electronics*, vol. 54, no. 1, pp. 530–538, Feb. 2007.

[9] N. C. Zhao B, "Estimating tool–tissue forces using a 3-degree-of-freedom robotic surgical tool," *ASME. J. Mech. Robot.*, vol. 8, no. 5, 2016, Art. no. 0510151.

[10] M. Khoshnam, A. C. Skanes, and R. V. Patel, "Modeling and estimation of tip contact force for steerable ablation catheters," *IEEE Trans. Biomed. Eng.*, vol. 62, no. 5, pp. 1404–1415, May 2015.

[11] E. Berger, "Friction modeling for dynamic system simulation," *Appl. Mech. Rev.*, vol. 55, no. 6, pp. 535–577, 2002.

[12] F. Anooshahpour, I. G. Polushin, and R. V. Patel, "Quasi-static modeling of the da Vinci instrument," in *Proc. IEEE/RSJ Int. Conf. Intell. Robots Syst.* IEEE, 2014, pp. 1308–1313.

[13] W. T. Townsend, "The effect of transmission design on force-controlled manipulator performance," Ph.D. dissertation, Dept. Mech. Eng., Mass. Inst. of Technol., Cambridge, MA, 1988.

[14] M. Miyasaka, M. Haghighipanah, Y. Li, and B. Hannaford, "Hysteresis model of longitudinally loaded cable for cable drivenrobots and identification of the parameters," in *Proc. IEEE Int. Conf. Robot. Autom.*, 2016, pp. 4051–4057.

[15] A. L. Muneaki Miyasaka, J. Matheson, and B. Hannaford, "Measurement of the cable-pulley coulomb and viscous friction for acable-driven surgical robotic system," in *Proc. Int. Conf. Intell. Robots Syst.*, Hamburg, German, Oct. 2015, pp. 804–810.

[16] Y. Li, M. Miyasaka, M. Haghighipanah, L. Cheng, and B. Hannaford, "Dynamic modeling of cable driven elongated surgical instruments forsensorless grip force estimation," in *Proc. IEEE Int. Conf. Robot. Autom.*, 2016, pp. 4128–4134.

[17] C. E. Rasmussen, *Gaussian Processes in Machine Learning*. Berlin, Heidelberg, Germany: Springer, 2004, pp. 63–71.

[18] B. Hannaford *et al.*, "Raven-II: An open platform for surgical robotics research," *IEEE Trans. Biomed. Eng.*, vol. 60, no. 4, pp. 954–959, Apr. 2013.

[19] C. M. Bishop, "Pattern recognition," *Mach. Learn.*, vol. 128, pp. 607–646, 2006.

[20] E. A. Wan and R. Van Der Merwe, "The unscented Kalman filter for nonlinear estimation," in *Proc. Adaptive Syst. Signal Process., Commun. Control Symp*. IEEE, 2000, pp. 153–158.

[21] I. R. Manchester and J.-J. E. Slotine, "Output-feedback control of nonlinear systems using control contraction metrics and convex optimization," in *Proc. 4th Australian Control Conf.* IEEE, 2014, pp. 215–220.

[22] M. Haghighipanah, M. Miyasaka, Y. Li, and B. Hannaford, "Unscented Kalman filter and 3d vision to improve cable driven surgical robot joint angle estimation," in *Proc. 2016 IEEE Int. Conf. Robot. Autom*. IEEE, 2016, pp. 4135–4142.

[23] J. Ko, D. J. Klein, D. Fox, and D. Haehnel, "Gp-ukf: Unscented kalman filters with gaussian process prediction and observation models," in *Proc. IEEE/RSJ Int. Conf. Intell. Robots Syst*. IEEE, 2007, pp. 1901–1907.

[24] L. Cheng, "Computation and measurement of force and tissue damage for the grasper-tissue interface in robot-assisted minimal invasive surgery," Ph.D. dissertation, Dept. Mech. Eng., Univ. Washington, 2015.

[25] Y. Li and E. B. Olson, "Extracting general-purpose features from LiDAR data," in *Proc. IEEE Int. Conf. Robot. Autom*. IEEE, 2010, pp. 1388–1393.

[26] M. P. Deisenroth, D. Fox, and C. E. Rasmussen, "Gaussian processes for data-efficient learning in robotics and control," *IEEE Trans. Pattern Anal. Mach. Intell.*, vol. 37, no. 2, pp. 408–423, Feb. 2015.